9-10-2012

Subwavelength ripples adjustment based on electron dynamics control by using shaped ultrafast laser pulse trains

Lan Jiang
Beijing Institute of Technology, jianglan@bit.edu.cn

Xuesong Shi
Beijing Institute of Technology

Xin Li
Beijing Institute of Technology

Yanping Yuan
Beijing Institute of Technology

Cong Wang
Beijing Institute of Technology

See next page for additional authors

Subwavelength ripples adjustment based on electron dynamics control by using shaped ultrafast laser pulse trains

Lan Jiang,[1,*] Xuesong Shi,[1] Xin Li,[1] Yanping Yuan,[1] Cong Wang,[1] and Yongfeng Lu[2]

[1]*NanoManufacturing Fundamental Research Joint Laboratory of National Science Foundation of China, School of Mechanical Engineering, Beijing Institute of Technology, Beijing 100081, People's Republic of China*
[2]*Department of Electrical Engineering, University of Nebraska-Lincoln, Lincoln, NE 68588-0511, USA*
[*]*jianglan@bit.edu.cn*

Abstract: This study reveals that the periods, ablation areas and orientations of periodic surface structures (ripples) in fused silica can be adjusted by using designed femtosecond (fs) laser pulse trains to control transient localized electron dynamics and corresponding material properties. By increasing the pulse delays from 0 to 100fs, the ripple periods are changed from ~550nm to ~255nm and the orientation is rotated by 90°. The nearwavelength/subwavelength ripple periods are close to the fundamental/second-harmonic wavelengths in fused silica respectively. The subsequent subpulse of the train significantly impacts free electron distributions generated by the previous subpulse(s), which might influence the formation mechanism of ripples and the surface morphology.

OCIS codes: (140.3390) Laser materials processing; (140.7090) Ultrafast lasers; (050.6624) Subwavelength structures.

References and links

1. M. Birnbaum, "Semiconductor surface damage produced by ruby lasers," J. Appl. Phys. **36**(11), 3688–3689 (1965).
2. J. F. Young, J. S. Preston, H. M. van Driel, and J. E. Sipe, "Laser-induced periodic surface structure. II. Experiments on Ge, Si, Al, and brass," Phys. Rev. B **27**(2), 1155–1172 (1983).
3. Y. F. Lu, W. K. Choi, Y. Aoyagi, A. Kinomura, and K. Fujii, "Controllable laser-induced periodic structures at silicon-dioxide/silicon interface by excimer laser irradiation," J. Appl. Phys. **80**(12), 7052–7056 (1996).
4. J. Wang and C. Guo, "Ultrafast dynamics of femtosecond laser-induced periodic surface pattern formation on metals," Appl. Phys. Lett. **87**(25), 251914 (2005).
5. R. Le Harzic, H. Schuck, D. Sauer, T. Anhut, I. Riemann, and K. König, "Sub-100 nm nanostructuring of silicon by ultrashort laser pulses," Opt. Express **13**(17), 6651–6656 (2005).
6. M. Couillard, A. Borowiec, H. K. Haugen, J. S. Preston, E. M. Griswold, and G. A. Botton, "Subsurface modifications in indium phosphide induced by single and multiple femtosecond laser pulses: A study on the formation of periodic ripples," J. Appl. Phys. **101**(3), 033519 (2007).
7. J. Gottmann, D. Wortmann, and M. Hörstmann-Jungemann, "Fabrication of sub-wavelength surface ripples and in-volume nanostructures by fs-laser induced selective etching," Appl. Surf. Sci. **255**(10), 5641–5646 (2009).
8. A. Borowiec and H. K. Haugen, "Subwavelength ripple formation on the surfaces of compound semiconductors irradiated with femtosecond laser pulses," Appl. Phys. Lett. **82**(25), 4462–4464 (2003).
9. D. C. Emmony, R. P. Howson, and L. J. Willis, "Laser mirror damage in germanium at 10.6 μm," Appl. Phys. Lett. **23**(11), 598–600 (1973).
10. Y. Shimotsuma, P. G. Kazansky, J. R. Qiu, and K. Hirao, "Self-Organized Nanogratings in glass irradiated by ultrashort light pulses," Phys. Rev. Lett. **91**(24), 247405 (2003).
11. V. R. Bhardwaj, E. Simova, P. P. Rajeev, C. Hnatovsky, R. S. Taylor, D. M. Rayner, and P. B. Corkum, "Optically produced arrays of planar nanostructures inside fused silica," Phys. Rev. Lett. **96**(5), 057404 (2006).
12. T. Q. Jia, H. X. Chen, M. Huang, F. L. Zhao, J. R. Qiu, R. X. Li, Z. Z. Xu, X. K. He, J. Zhang, and H. Kuroda, "Formation of nanogratings on the surface of a ZnSe crystal irradiated by femtosecond laser pulses," Phys. Rev. B **72**(12), 125429 (2005).

#170111 - $15.00 USD Received 8 Jun 2012; revised 9 Jul 2012; accepted 21 Aug 2012; published 5 Sep 2012

13. J. W. Yao, C. Y. Zhang, H. Y. Liu, Q. F. Dai, L. J. Wu, S. Lan, A. V. Gopal, V. A. Trofimov, and T. M. Lysak, "High spatial frequency periodic structures induced on metal surface by femtosecond laser pulses," Opt. Express **20**(2), 905–911 (2012).
14. E. M. Hsu, T. H. R. Crawford, H. F. Tiedje, and H. K. Haugen, "Periodic surface structures on gallium phosphide after irradiation with 150 fs-7 ns laser pulses at 800nm," Appl. Phys. Lett. **91**(11), 111102 (2007).
15. J. Bonse, M. Munz, and H. Sturm, "Structure formation on the surface of indium phosphide irradiated by femtosecond laser pulses," J. Appl. Phys. **97**(1), 013538 (2005).
16. M. Huang, F. L. Zhao, Y. Cheng, N. S. Xu, and Z. Z. Xu, "The morphological and optical characteristics of femtosecond laser-induced large-area micro/nanostructures on GaAs, Si, and brass," Opt. Express **18**(S4 Suppl 4), A600–A619 (2010).
17. L. Jiang and H. L. Tsai, "Repeatable nanostructures in dielectrics by femtosecond laser pulse trains," Appl. Phys. Lett. **87**(15), 151104 (2005).
18. V. Hommes, M. Miclea, and R. Hergenröder, "Silicon surface morphology study after exposure to tailored femtosecond pulses," Appl. Surf. Sci. **252**(20), 7449–7460 (2006).
19. J. Kim, S. Na, S. Cho, W. Chang, and K. Whang, "Surface ripple changes during Cr film ablation with a double ultrashort laser pulse," Opt. Lasers Eng. **46**(4), 306–310 (2008).
20. A. Rosenfeld, M. Rohloff, S. Höhm, J. Krüger, and J. Bonse, "Formation of laser-induced periodic surface structures on fused silica upon multiple parallel polarized double-femtosecond-laser-pulse irradiation sequences," Appl. Sur. Sci. doi: 10.1016/j.apsusc.2011.09.076 (2011).
21. M. Li, S. Menon, J. P. Nibarger, and G. N. Gibson, "Ultrafast electron dynamics in femtosecond optical breakdown of dielectrics," Phys. Rev. Lett. **82**(11), 2394–2397 (1999).
22. R. Stoian, M. Boyle, A. Thoss, A. Rosenfeld, G. Korn, I. V. Hertel, and E. E. B. Campbell, "Laser ablation of dielectrics with temporally shaped femtosecond pulses," Appl. Phys. Lett. **80**(3), 353–355 (2002).
23. R. Stoian, M. Boyle, A. Thoss, A. Rosenfeld, G. Korn, and I. V. Hertel, "Dynamic temporal pulse shaping in advanced ultrafast laser material processing," Appl. Phys., A Mater. Sci. Process. **77**(2), 265–269 (2003).
24. G. Sansone, E. Benedetti, F. Calegari, C. Vozzi, L. Avaldi, R. Flammini, L. Poletto, P. Villoresi, C. Altucci, R. Velotta, S. Stagira, S. De Silvestri, and M. Nisoli, "Isolated single-cycle attosecond pulses," Science **314**(5798), 443–446 (2006).
25. A. L. Cavalieri, N. Müller, Th. Uphues, V. S. Yakovlev, A. Baltuška, B. Horvath, B. Schmidt, L. Blümel, R. Holzwarth, S. Hendel, M. Drescher, U. Kleineberg, P. M. Echenique, R. Kienberger, F. Krausz, and U. Heinzmann, "Attosecond spectroscopy in condensed matter," Nature **449**(7165), 1029–1032 (2007).
26. E. Goulielmakis, V. S. Yakovlev, A. L. Cavalieri, M. Uiberacker, V. Pervak, A. Apolonski, R. Kienberger, U. Kleineberg, and F. Krausz, "Attosecond control and measurement: lightwave electronics," Science **317**(5839), 769–775 (2007).
27. C. Wang, L. Jiang, F. Wang, X. Li, Y. P. Yuan, and H. L. Tsai, "First-principles calculations of the electron dynamics during femtosecond laser pulse train material interactions," Phys. Lett. A **375**(36), 3200–3204 (2011).
28. L. Jiang, P. J. Liu, X. L. Yan, N. Leng, C. C. Xu, H. Xiao, and Y. F. Lu, "High-throughput rear-surface drilling of microchannels in glass based on electron dynamics control using femtosecond pulse trains," Opt. Lett. **37**(14), 2781–2783 (2012).
29. M. Shinoda, R. R. Gattass, and E. Mazur, "Femtosecond laser-induced formation of nanometer-width grooves on synthetic single-crystal diamond surfaces," J. Appl. Phys. **105**(5), 053102 (2009).
30. R. Buividas, L. Rosa, R. Šliupas, T. Kudrius, G. Šlekys, V. Datsyuk, and S. Juodkazis, "Mechanism of fine ripple formation on surfaces of (semi) transparent materials via a half-wavelength cavity feedback," Nanotechnology **22**(5), 055304 (2011).
31. L. Jiang and H. L. Tsai, "Plasma modeling for ultrashort pulse laser ablation of dielectrics," J. Appl. Phys. **100**(2), 023116 (2006).
32. Y. P. Yuan, L. Jiang, X. Li, C. Wang, H. Xiao, Y. F. Lu, and H. L. Tsai, "Formation mechanisms of sub-wavelength ripples during femtosecond laser pulse train processing of dielectrics," J. Phys. D **45**(17), 175301 (2012).
33. F. Liang, R. Vallée, and S. L. Chin, "Mechanism of nanograting formation on the surface of fused silica," Opt. Express **20**(4), 4389–4396 (2012).

1. Introduction

Laser-induced periodic surface structures (LIPSS/ripples) have attracted tremendous attention for many years [1–8]. LIPSS can be divided into two distinct types: low spatial frequency LIPSS (LSFL) and high spatial frequency LIPSS (HSFL) [8]. LSFL consist of spatial periods (Λ) close to the irradiation wavelength (λ, $\lambda > \Lambda > \lambda/2$), which are widely considered to be the result of the interaction between an incident wave and a surface scattered wave [2,9]. The

#170111 - $15.00 USD Received 8 Jun 2012; revised 9 Jul 2012; accepted 21 Aug 2012; published 5 Sep 2012

spatial periods of HSFL are significantly smaller than the irradiation laser wavelength ($\Lambda<\lambda/2$), and their formation mechanism is still under investigation [10–13]. The effects of the pulse duration [14], pulse number [15], and fluence [16] on the evolution of LIPSS are all studied. For femtosecond (fs) laser pulse train processing of materials, the pulse delay between subpulses also strongly impacts the formation of nanostructures [17–20], especially the morphology of LIPSS [18–20]. Rosenfeld et al. [20] found that HSFL began to appear at a pulse delay of 1.33ps and completely replaced LSFL at 40ps, which was attributed to the free-electron plasma generation and transient changes of the optical properties during the ablation process. More detailed studies in the femtosecond timescale are still required to reveal the fundamental formation mechanisms of LIPSS within the ultrafast carrier lifetime (a few to hundreds of 100fs) [21–23] for fs laser-induced dense plasma in fused silica. In addition, the control of the LIPSS morphology, such as periods, areas and orientations, still remains a challenge.

On the other hand, a fs pulse duration is shorter than many physical/chemical characteristic times, which enables it to manipulate/adjust/interfere electron dynamics, such as excitation, ionization, recombination in addition to density and temperature of the electrons [24–26]. Recently, we proposed that transient localized electron dynamics could be controlled to adjust corresponding material properties by shaping fs pulse trains for high-precision nanostructuring [27]. This was experimentally validated by drilling high-aspect-ratio microchannels in glass using shaped fs pulse trains [28]. Hence, the control of LIPSS formation becomes possible by designing fs pulse trains according to transient localized electron dynamics during the ablation process.

In this study, the topography evolution of LIPSS is investigated by 50fs, 800 nm laser pulse trains at different pulse delays, Δt, from 0 to 1ps. Abrupt transitions from LSFL to HSFL at pulse delays within 100fs under certain conditions are observed for the first time. The experiments demonstrate that it is feasible to control the LIPSS morphology, such as periods, areas and orientations, by carefully designing pulse trains according to transient localized electron dynamics, for which fundamental insights of LIPSS formation mechanisms are presented.

2. Experimental set-up

A 3.5W fs Ti:sapphire laser (Spectra Physics, Inc.) is used to generate linearly polarized laser pulses of 50fs (FWHM) pulse duration at 800nm central wavelength. The fused silica sample is mechanically polished to a surface roughness of 0.5nm Ra and mounted on a six-axis translation stage. Desired pulse trains are generated by a commercial 4f-configuration-based pulse shaper (BSI MIIPS BOX 640), which allows the adjustment of delay times ranging from 4fs to 5ps. By scaling the laser repetition rate down to 10Hz, the number of bursts per site (N) is precisely controlled with an electromechanical shutter, in which a burst is defined as the irradiation of a whole pulse train. The p-polarized laser beam is incident normal to the sample surface by a 5 × microscope objective (N.A. = 0.1, Olympus), corresponding to a spot size diameter of ~8μm. A half-wave plate and polarizer, mounted prior to the entrance of the pulse shaper, are used to adjust the total energy of the pulse train. The pulse train in our experiments consists of two subpulses, and the intensity ratio is 1:1. All experiments are carried out in air at ambient pressure and temperature. After irradiation, the surface morphology is investigated by a scanning electron microscope (SEM) and an atomic force microscope (AFM).

3. Results and discussion

For multiple laser pulses irradiation (pulse delay $\Delta t = 0$), the types of LIPSS strongly depend on the fluencies and the pulse numbers (N_0). At N_0 = 5-50, LSFL with orientation parallel to the laser polarization can be obtained at $0.72F_{th}$-$3F_{th}$, in which F_{th} is the single-pulse threshold

#170111 - $15.00 USD Received 8 Jun 2012; revised 9 Jul 2012; accepted 21 Aug 2012; published 5 Sep 2012

fluence. F_{th} is the minimal fluence for a single pulse that just creates the visible damage on the sample surface observed by the CCD imaging system. The periods of LSFL at N_0 = 5-50 are 800-540 nm and decrease with the increase in N_0. However, HSFL, orientated perpendicular to the polarization, are pronounced only at fluencies in the range of $0.6F_{th}$-$0.66F_{th}$ at N_0>15. Although the parameters of processing LSFL are so different than those for HSFL, both types of ripples can be obtained by changing the pulse delay (Δt) at fixed total fluence and number of pulse trains (N).

3.1 The periods and areas of LSFL

An interesting phenomenon of the decrease of the areas and periods of LSFL can be observed by varying pulse delays at the fluences of $1F_{th}$-$1.05F_{th}$. Figure 1 shows LSFL and HSFL after irradiation with N = 10 pulse trains at $1.05F_{th}$. By increasing pulse delays from 0 to 50fs, two types of LIPSS are obtained in which 0fs is considered as a train consisting of two pulses at half of total fluence with zero pulse delay. At zero pulse delay, Δt = 0fs, regular LSFL and the separations of several peaks are observed in the overall ablation area as shown in Fig. 1(a) and the corresponding enlarged image. At Δt = 50fs, the ablation area significantly decreases; and the peaks of LSFL are split, where the HSFL (parallel to LSFL), with periods approximately half of that of the LSFL, are obtained in Fig. 1(b). Some nanostructures (perpendicular to the polarization) on the rim of the ablation crater can also be observed in the enlarged image of Fig. 1(b). At Δt>50fs, no obvious structures are obtained. The average periods of LSFL and HSFL are 560 ± 8nm and 255 ± 10nm, respectively, while λ/n = 551nm and λ/2n = 275nm (λ is the incident central wavelength and n is the refractive index). The periods of LSFL and HSFL are close to the fundamental and second-harmonic wavelengths in the fused silica. This indicates that the second-harmonic generation (SHG) plays a key role in triggering the LIPSS transition at a pulse delay of 50fs. The SHG is also proposed to explain the formation of HSFL in semiconductors [8,12,15]. The harmonics, resulting from electron recombination, are determined by the occupation of excited electrons in a conduction band. The electron occupation can be adjusted by shaping a fs pulse train, which was theoretically predicted by us [27]. Thus, the changes in electron occupation might facilitate SHG and result in a 50% cut in ripple periods. On the other hand, the strong decrease in the ablation area is due to the electron decay during the pulse delay at lower intensity regions of the laser spot [22].

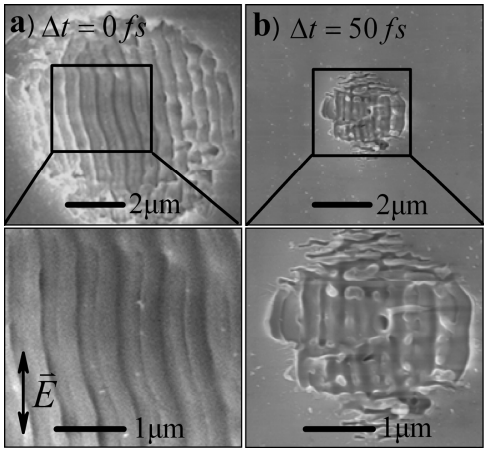

Fig. 1. SEM images of LIPSS morphology evolution on fused silica surface after irradiation with 10 pulse trains (two pulses per train) at a total fluence of $1.05F_{th}$. The polarization direction is indicated by the arrow.

#170111 - $15.00 USD Received 8 Jun 2012; revised 9 Jul 2012; accepted 21 Aug 2012; published 5 Sep 2012

3.2 Transition from LSFL to HSFL

With higher fluences ($1.1F_{th}$-$1.22F_{th}$) and more pulse trains (N = 20), LSFL are replaced by another type of HSFL (orientated perpendicular to LSFL and with laser polarization) at $\Delta t \geq 100$fs. Figure 2 shows the transition from LSFL to HSFL after irradiation with N = 20 pulse trains at $1.16F_{th}$. At Δt = 0fs, LSFL, orientated parallel to the laser polarization, are regularly distributed on the bottom of the ablation crater (Fig. 2(a)). At Δt = 50fs (Fig. 2(b)), the rippled area decreases rapidly; and LSFL only exist in the central crater region. In a pulse delay range of 100fs to 400fs (Δt = 100-400fs) (Figs. 2(c)-2(f)), typical nanostructures of HSFL, with orientation perpendicular to laser polarization, become dominant. The periods of HSFL at 100fs delay are 255 ± 30nm. No obvious structures are formed at Δt>500fs. In order to gain more information on the morphological characteristics, AFM is used to investigate both LSFL and HSFL. The profiles of the periodic structures in Figs. 2(a) and 2(f) are shown in Figs. 3(a) and 3(b), respectively. It is found that after irradiation by pulse trains: 1) the depth of the ablation crater significantly decreases as the pulse delay increases; 2) LSFL are replaced by HSFL on the surface; 3) the spatial periods of the LIPSS strongly decrease; and 4) the orientation of HSFL rotates by 90° to be perpendicular to that of LSFL and the laser polarization.

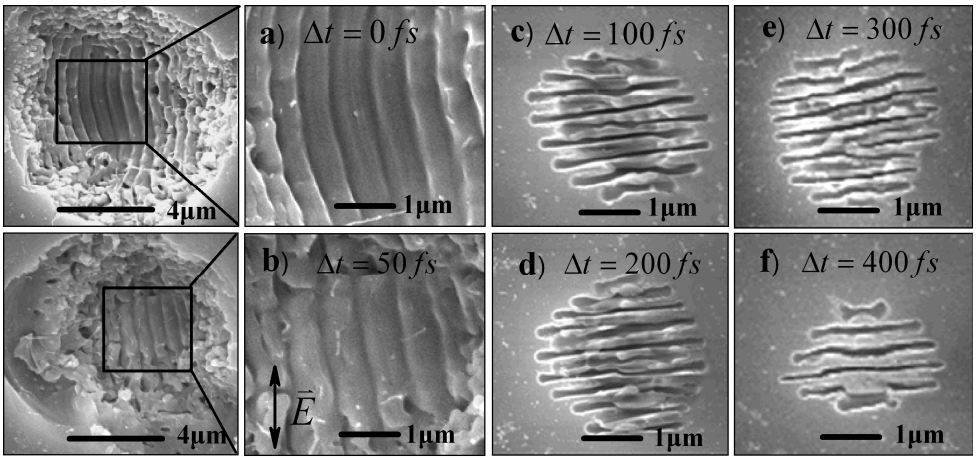

Fig. 2. LSFL and HSFL at a pulse delay of (a) 0fs, (b) 50fs, (c) 100fs, (d) 200fs, (e) 300fs and (f) 400fs after irradiation with 20 pulse trains (two pulses per train) at a total fluence of $1.16F_{th}$. The polarization direction is indicated by the arrow.

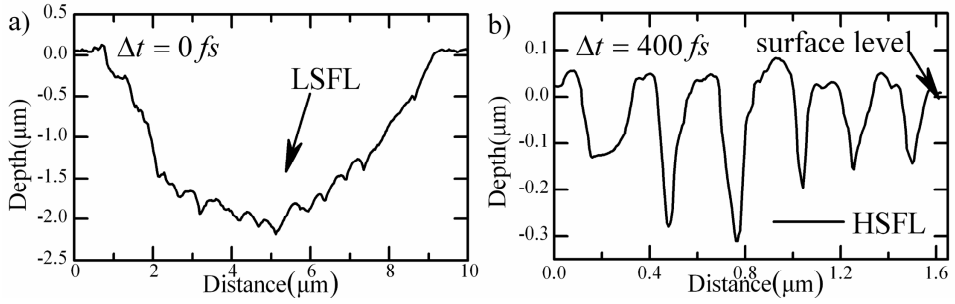

Fig. 3. (a) AFM profile of LSFL in Fig. 2(a). The LSFL are observed at the bottom of the ablated crater. (b) AFM profile of HSFL in Fig. 2(f).

#170111 - $15.00 USD Received 8 Jun 2012; revised 9 Jul 2012; accepted 21 Aug 2012; published 5 Sep 2012

3.3 Effects of pulse delay on the LIPSS transition

Effects of pulse delay on the spatial periods and ablation areas of LIPSS at the total fluence of $1.16F_{th}$ are shown in Fig. 4, where the error bar indicates the measurement errors and the spatial nonuniformity of the structures. As shown in Fig. 4, within $\Delta t \leq 100$fs, the periods and ablation areas of LIPSS decrease rapidly, whereas from 100fs onwards, they become stable. For multiple pulses (Δt = 0fs) irradiation, the previous pulses increase the incident angle and surface roughness at the rim of the crater for subsequent pulses; and LSFL are established from the edge to the overall ablation area. As the pulse delay increases, a single pulse is separated into two delayed subpulses; and neither of them is sufficient to damage the surface. Structures [29,30] on the dielectrics surface are very similar to the HSFL described in this work, which can be attributed to the periodic plasma enhancement of the incident laser field at the surface [29]. During the ablation process, surface plasmons can be resonantly excited by coupling between the surface free electrons and the incident field at a certain electron density. At a pulse delay of 0fs, after the free electron density becomes comparable to the critical density, the laser energy is mainly reflected; and the Gaussian beam is strongly reshaped [31]. Hence, the intensity of the absorbed laser is low; and the effects of induced surface plasmons on the incident laser are not sufficient. As to pulse delays in the range of 100fs-500fs, however, surface plasmons excitation can easily be achieved at the initial stage of the second subpulse due to accumulation of the first subpulse [32]. Because of the interaction between the incident laser field and surface plasmons, the coupled field intensity is enhanced in some areas and weakened in others with spatially periodic patterns at the surface. Combined with multiple bursts irradiation, the incubation effects result in the evolution of local intensity distribution along the electric field direction [33]. Energy with such patterns leads to periodic distributions of the free electron density, forming HSFL at a specific periodicity and an orientation perpendicular to the electric field direction. Thus, by designing a fs laser pulse train based on transient localized electron dynamics and corresponding material properties: 1) the electron dynamics can be controlled; 2) the interaction time between the surface plasmons and the incident field is prolonged and 3) ripples with different periods and orientations can be obtained.

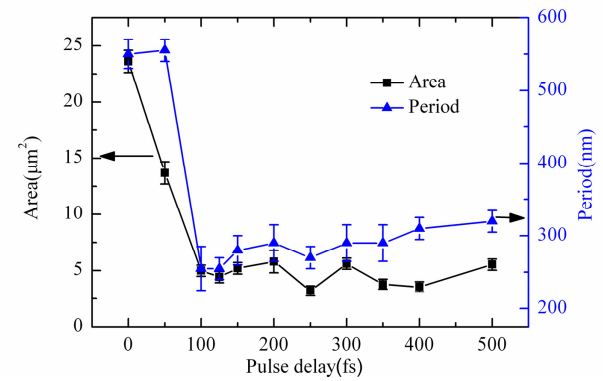

Fig. 4. Periods and areas of LIPSS as a function of pulse delay by 20 pulse trains (two pulses per train) at the total fluence of $1.16F_{th}$.

In the overall ablation process, free electron decay is inevitable; and the details of free electron decay time are explained in [17]. Similarly, an ultrafast carrier lifetime in fs regime (~100fs) for fused silica has been demonstrated by several studies [21–23]. With an increasing pulse delay, the electronic decay strongly impacts the density of free electrons, which leads to less seed electrons and inhibits ionization in the overall process. Hence, smaller ablation areas and depths are obtained at pulse delays of 50-100fs (as shown in Fig. 4).

#170111 - $15.00 USD Received 8 Jun 2012; revised 9 Jul 2012; accepted 21 Aug 2012; published 5 Sep 2012

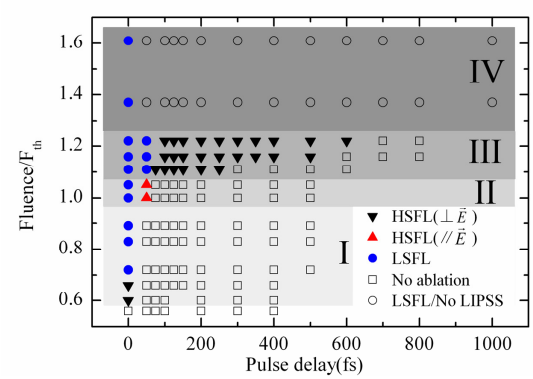

Fig. 5. Different fluence regions of the types of surface morphology as functions of pulse delay in fused silica after multiple bursts irradiation. ("Fluence/F_{th}" represents the ratio of the total fluence to the single-pulse threshold fluence; "O" signifies LSFL at N = 10 and represents disorganized structures at N>10).

Figure 5 summarizes the types of ripples as functions of the pulse delay in four fluence regions. In region I, HSFL($\perp \vec{E}$) and LSFL are obtained at 0fs pulse delay (single pulse) after tens of laser pulses irradiation. HSFL are quite sensitive to the N variations in the range of $0.6F_{th}$-$0.66F_{th}$; and are pronounced only at specific combinations of the two parameters (fluence and N). In region II, the increasing of the pulse delay results in a 50% cut in LSFL periods and HSFL($// \vec{E}$) are obtained, which is probably due to the SHG. This region is of practical importance for the reduction of LSFL periods. In region III, the transition from LSFL to HSFL($\perp \vec{E}$) is achieved and found to associate LIPSS orientation rotating at pulse delays in the range of 75-100fs, which is attributed to the interaction between the surface plasmons and incident field. In this region, by increasing the pulse delays between the subpulses in a train with fixed N and fluence, the types of LIPSS can be controlled, which provides a feasible method to control the ripple type and orientation towards the polarization. In region IV, LSFL are dominant structures if N = 10 and no LIPSS is observed if N>10.

4. Conclusions

In summary, the topography evolution of LIPSS in fused silica by fs pulse trains has been investigated. It is found that: 1) at $1F_{th}$-$1.05F_{th}$ fluence and N = 10, LSFL are obtained at pulse delay Δt = 0fs and split in the peaks at Δt = 50fs, leading to additional HSFL orientated parallel to LSFL and laser polarization. The periods of LSFL and those of HSFL are close to the fundamental and second-harmonic wavelengths in the fused silica, respectively, which indicates that the second-harmonic generation is the key in triggering the LIPSS transition at Δt = 50fs; 2) at higher fluences of $1.1F_{th}$-$1.22F_{th}$ and N = 20, LSFL, obtained at Δt = 0fs, are replaced by orthotropic HSFL at Δt = 75-600fs, which is attributed to surface plasmons generation and the periodic enhancement of the coupled electric field at the surface. The experimental results demonstrate that localized transient electron dynamics play an important role in LIPSS formation, which can be adjusted by the pulse train. The dependence of the LIPSS morphology on the pulse delay provides a new method to obtain controllable and smaller nanogratings.

Acknowledgments

This research is supported by the National Basic Research Program of China (973 Program) (Grant No. 2011CB013000) and National Natural Science Foundation of China (NSFC) (Grant Nos. 90923039 and 51025521).

#170111 - $15.00 USD Received 8 Jun 2012; revised 9 Jul 2012; accepted 21 Aug 2012; published 5 Sep 2012